An investigation on causes of the detected surface solar radiation brightening in Europe using satellite data

Linda Schilliger[1,2], Anke Tetzlaff[1], Quentin Bourgeois[1], Lucas Ferreira Correa[2], and Martin Wild[2]

[1]Federal Office for Meteorology and Climatology (MeteoSwiss), Zurich, Switzerland
[2]Institute for Atmospheric and Climate Science, ETH Zurich, Zurich, Switzerland

Key Points:

- CM SAF Land Flux v1.0 surface solar radiation data agree well with station-based measurements over Europe, also at high-altitude locations.
- The direct aerosol effect was the main driver of the European brightening from 1983 to 2000. Changes in cloudiness rather counteracted it.
- After 2000 the brightening in Europe was dominated by the cloud effect, whereas the aerosol effect resulted rather negligible.

Corresponding author: Linda Schilliger, linda.schilliger@meteoswiss.ch

Abstract

Surface solar radiation is fundamental for terrestrial life. It provides warmth to make our planet habitable, drives atmospheric circulation, the hydrological cycle and photosynthesis. Europe has experienced an increase in surface solar radiation, termed "brightening", since the 1980s. This study investigates the causative factors behind this brightening. A novel algorithm from the EUMETSAT satellite application facility on climate monitoring (CM SAF) provides the unique opportunity to simulate surface solar radiation under various atmospheric conditions for clouds (clear-sky or all-sky), aerosol optical depth (time-varying or climatological averages) and water vapor content (with or without its direct influence on surface solar radiation). Through a multiple linear regression approach, the study attributes brightening trends to changes in these atmospheric parameters. Analyzing 61 locations distributed across Europe from 1983 to 2020, aerosols emerge as key driver during 1983-2002, with Southern Europe and high elevations showing subdued effects (0-1%/decade) versus more pronounced impacts in Northern and Eastern Europe (2-6%/decade). Cloud effects exhibit spatial variability, inducing a negative effect on surface solar radiation (-3 to -2%/decade) at most investigated locations in the same period. In the subsequent period 2001-2020, aerosol effects are negligible, while cloud effects dominate the observed brightening (2-5%/decade). This study therefore finds a substantial decrease in the cloud radiative forcing over Europe in the first two decades of the 21st century. Water vapor exerts negligible influence in both sub-periods.

Plain Language Summary

This study explores the recent increase in surface solar radiation in Europe, commonly referred to as "brightening", which began in the mid-1980s. Surface solar radiation is crucial for life on Earth, fostering warmth, shaping wind patterns, and fueling the hydrological cycle and photosynthesis. Utilizing data derived from satellites, we simulated surface solar radiation under different atmospheric conditions regarding clouds, aerosols, and water vapor. This allowed us to separate the individual effects and analyze their contributions to the observed brightening across 61 locations in Europe from 1983 to 2020. We find that the decrease in aerosols was the dominant driver for the brightening during the initial period from 1983 to 2002. Southern Europe and high-elevation areas showed modest aerosol effects, while Northern and Eastern Europe experienced higher values. Cloud effects were predominantly negative (decreasing surface solar radiation) at most locations. However, between 2001 and 2020 the aerosol effect resulted negligible and the brightening was mostly attributed to a decrease in cloudiness during that subperiod. Water vapor was found to have a negligible impact on surface solar radiation trends.

1 Introduction

Solar radiation incident upon Earth's surface, also referred to as surface solar radiation or surface incoming solar radiation (SIS) represents the primary energy source for life on our planet. It governs a multitude of environmental processes. Not only does it provide heat directly to our environments, it also plays a crucial role in the global hydrological cycle by providing energy for evaporation, enabling photosynthesis, supporting plant growth, and inducing pressure gradients that influence atmospheric circulation patterns. Given its fundamental role in creating habitable environments, Earth is greatly sensitive to potential variations in surface solar radiation. This sensitivity extends to solar power generation, as solar power plants are receiving strong interest due to their potential as renewable energy sources (Wild, 2012; Jacobson & Delucchi, 2011; Zou et al., 2019). Due to being of such high importance for numerous essential processes, the analysis of surface solar radiation trends and their causes is crucial. Several studies (e.g., Ohmura, 1989; Stanhill & Moreshet, 1992; Liepert, Fabian, & Grassl, 1994; Gilgen, Wild, & Ohmura, 1998; Gilgen, Roesch, Wild, & Ohmura, 2009; Sanchez-Lorenzo et al., 2015) have found a negative surface solar radiation trend (dimming) over land regions until the mid-1980s, spanning approximately three decades. Studies have found indications of a weakened hydrological cycle (e.g., Liepert, Feichter, Lohmann, & Roeckner, 2004; Liepert & Romanou, 2005) and a reduction of

the diurnal surface temperature range (Wild et al., 2007) during this dimming phase. Furthermore, this dimming has masked the global warming to some extent (Murphy et al., 2009; Wild et al., 2007; Wild, 2016). More recent studies have further highlighted the importance of quantifying surface solar radiation trends by finding the shortwave warming to be a larger contributor to the global warming than the long-wave warming (greenhouse effect) (Philipona et al., 2009). From around 1985 up to recent times a positive trend (brightening) has been found at many locations (Wild et al., 2005; Gilgen et al., 2009; Sanchez-Lorenzo et al., 2015). However, the brightening period is not as globally discovered as the dimming period (e.g., no brightening in India, Padma Kumari & Goswami, 2010; Wild, 2009). After 2000, the brightening has exhibited reduced intensity in some regions, such as China and Japan. In contrast, Europe and the USA have experienced continued brightening, albeit with some indications of stabilization in recent years (Wild et al., 2005, 2021).

As the surface solar radiation variability is larger than the variability of the solar output, global dimming and brightening cannot be explained by variations in extraterrestrial solar irradiance (Foukal et al., 2006), making Earth's atmosphere responsible for them. In dimming times, the atmosphere is more opaque and therefore more solar radiation is reflected back to space and less is let through the atmosphere towards Earth's surface, eventually cooling Earth. Less reflection and more solar radiation coming through the atmosphere heat up Earth's surface during brightening times. Changes in atmospheric aerosol concentration or clouds have been suggested as causes of dimming and brightening periods. The majority of studies come to the conclusion that changes in aerosol particle concentration in the atmosphere were the main driver of the recent positive surface solar radiation trends (Wild et al., 2005; Norris & Wild, 2007; Ruckstuhl et al., 2008; Ohvril et al., 2009; Philipona et al., 2009; Zerefos et al., 2009; Folini & Wild, 2011; Nabat et al., 2014; Wild et al., 2021; Julsrud et al., 2022; Zhou et al., 2023; Dong et al., 2023). Aerosol optical depth is majorly influenced by anthropogenic emissions, especially sulfur and also black carbon (Streets et al., 2009). Vestreng et al. (2007) reported a 60% decrease in sulfur emissions (one of the most abundant aerosol particles in the atmosphere) between 1990 and 2004 in Europe, supporting the theory of an important aerosol effect on the observed brightening during this period. However, recent analysis of satellite-derived data showed that the same trend is still visible when using a constant aerosol climatology, implying that only changes in cloudiness were responsible for the observed brightening from 1983 to 2010 (Sanchez-Lorenzo et al., 2017), respective from 1983 to 2015 (Pfeifroth et al., 2018). Additionally, focusing on the Iberian Peninsula and the period 2003 to 2012, Mateos et al. (2014) found a dominant cloud effect on surface solar radiation trends. Ferreira Correa et al. (2023) analyzed the Alpine region, while distinguishing between high and low elevation sites. They found strong evidence that, together with a surface albedo effect, changes in cloud optical depth were the primary effect causing the observed surface solar radiation trends at high elevation stations. At low elevation sites, however, they identified a strong aerosol effect causing the surface solar radiation trends.

Despite numerous investigations into this subject, the precise contributions of aerosols and clouds, along with their spatial distribution, remain unclear. This study endeavours to quantify the effects that have contributed to the recent brightening in Europe and to illustrate their geographic distribution utilizing newly generated satellite-derived data from the EUMETSAT Satellite Application Facility on Climate Monitoring (CM SAF). With the applied algorithm, it is possible to separate cloud, direct aerosol and water vapour effects by combining different simulations. In addition to analyzing the entire temporal span covering the period from 1983 to 2020, we scrutinize two distinct sub-periods: 1983 to 2020 and 2001 to 2020. This is motivated for two reasons: First, major efforts to reduce anthropogenic aerosol emissions took place in the 1980s and 1990s. Therefore, we consider the first sub-period as representative for the decline in anthropogenic aerosol particles and the second sub-period for more stable conditions. Second, the two sub-periods can also be dynamically justified, considering the decadal variability in the predominance of different atmospheric regimes. The initial sub-period is predominantly characterized by positive phases of the North Atlantic Oscillation (NAO), particularly during the 1990s. Positive NAO is generally associated with above-average precipitation and cloudiness. During the second sub-period NAO positive phases occurred less frequently and were less intense. In con-

trast, in particular winters around 2010 were dominated by negative phases of NAO, which are generally associated with less precipitation and cloudiness (Weisheimer et al., 2017; Papritz & Grams, 2018; Climate Prediction Center, 2024; National Weather Service - NOAA, 2024). The temporal split is robust and substantiated by supplementary material figures. We tested the sensitivity of the choice of the exact year for the split of the two sub-periods and found no substantial impact on our results (see Supplementary Material Figures S1 to S6).

2 Data

2.1 Satellite-Derived Data

This investigation utilized the CM SAF Meteosat Land Flux v1.0 Surface Radiation Budget (SRB) dataset (Bourgeois & Duguay-Tetzlaff, 2023), which was derived through the application of the "GeoSatClim" algorithm developed by MeteoSwiss to raw data sourced from the Meteosat satellite. This dataset encompasses all components of the SRB, including absorbed surface solar radiation, albedo, surface downward radiation, surface outgoing radiation, as well as latent and sensible heat fluxes, which were jointly retrieved with similar boundary conditions. Data is available for the period 1983/01/01 to 2020/12/31 with an hourly resolution and a spatial resolution of 0.05° x 0.05° longitude and latitude covering the geographic extent of ±75° longitude and ±75° latitude of the Meteosat disk.

The GeoSatClim software incorporates a physical retrieval scheme originally developed by Stoeckli (2017) and subsequently adapted to GeoSatClim by Bourgeois and Duguay-Tetzlaff (2023). With GeoSatClim, the Heliosat approach (Cano et al., 1986; Mueller et al., 2009) is expanded to encompass the infrared spectrum with the addition of a cloud optical depth calculation for both visible and infrared channels. These additional features enhance the performance, particularly in regions characterized by snow-covered mountains (Bourgeois & Duguay-Tetzlaff, 2023). The GeoSatClim SIS retrieval is entirely based on the new inter-calibrated Meteosat EUMETSAT radiances. Consequently, the decadal stability of the CM SAF Land Flux SIS is contingent on the quality of the new Meteosat calibration.

The computation of surface solar radiation requires cloud optical parameters, which are retrieved from the satellite, values of the atmospheric gas concentration, information about solar and viewing angles, the surface albedo, that is also retrieved by the satellite, and information about the aerosol optical depth (AOD). Time-varying aerosol optical depth information is taken from model-based estimates that include pre-industrial natural aerosol and emission estimates (Fiedler, Kinne, et al., 2019) and information on different emission scenarios (Fiedler, Stevens, et al., 2019). For the natural aerosols the monthly climatology MACv2 was used and the anthropogenic aerosol MACv2-SP information was considered for the period 1979 to 2014. The SSP2-45 emission scenario was utilized to model the anthropogenic aerosol optical depth for the period 2015 to 2020, since this data set was derived already some time ago. In addition to the tropospheric aerosols, stratospheric aerosol information from NASA GISS was incorporated (NASA, 2016). To generate the published CM SAF Land Flux data daily varying aerosols were used, thus accounting for the aerosol-induced brightening in the operational CM SAF Land Flux SIS data. Additionally, MeteoSwiss has generated SIS data employing an aerosol climatology using the CM SAF algorithm. The constant daily aerosol climatology is derived from the Copernicus Atmosphere Monitoring Service (CAMS) reanalysis produced by the European Centre for Medium-Range Weather Forecasts (ECMWF) (Inness et al., 2019). The AOD is bilinearly interpolated to the Meteosat grid from a 0.5° x 0.5° longitude and latitude resolution and temporally interpolated from 6-hour estimates to match the Meteosat temporal resolution. Moreover, a dataset devoid of direct influence from water vapor concentration on SIS was processed. The primary data utilized in this study comprises outputs generated by GeoSatClim, incorporating various configurations pertaining to clouds, aerosol input, and water vapor content. All analyses and subsequent conclusions drawn in this study are based exclusively on the examination of these datasets.

2.2 Station Data

To validate the satellite-derived data, data from the Global Energy Balance Archive (GEBA) (Wild et al., 2017) was employed for all locations beyond Switzerland. While the GEBA station data is not homogenized, datasets from Italy and Spain utilized in this study are derived from individually homogenized sources (Manara et al. (2016) for Italy, Sanchez-Lorenzo et al. (2013) for Spain). Norris and Wild (2007) demonstrated a strong agreement between ISCCP-FD (second generation of the International Satellite Cloud Climatology Project) all-sky flux and GEBA data on interannual timescales, affirming the reliability of GEBA measurements also on extended timescales. The GEBA data spans consistently from 1983/01/01 to 2015/12/31 across all considered locations, thereby restricting the validation of the satellite dataset to this timeframe. GEBA data, provided as monthly means, were processed according to protocols outlined on the WRDC (World Radiation Data Centre) website (`http://wrdc.mgo.rssi.ru/wrdc_en_new.htm`).

For validation within Switzerland, the newly homogenized ground measurements from MeteoSwiss (Swiss Met Net, SMN) were employed. These data provide monthly mean values for the period 1983/01/01 to 2020/12/31. Daily averages were calculated from instantaneous 10-minute measurements, with the aggregation of all daily means within a month yielding the monthly means. The averaging process tolerates 24 missing 10-minutes values for the daily means, with a constraint that no more than 14 consecutive missing values are permissible. In the most extreme scenario, this tolerance allows for the calculation of a daily mean even in the presence of a two-hour data gap around noon, which could potentially create a bias. Furthermore, when aggregating the daily to the monthly means, a maximum of 5 daily values can be absent with no more than 3 consecutive gaps tolerated.

For this investigation, a selection of 61 stations across Europe, providing continuous data, was chosen to serve as reference points in the validation procedure and for all further analysis. Among these stations 53 are located outside of Switzerland and were chosen as per table 1 in Pfeifroth et al. (2018). They checked the quality of the ground measurement data (GEBA) at these locations and they are relatively equally distributed covering different climate zones. In Switzerland a total of 8 stations was selected, including four low and four higher elevation locations. Very high altitude locations (altitude > 3000 meters) were excluded, as in mountainous (inhomogeneous) terrain area-wide satellite measurements cannot be compared to a point measurement.

3 Methodology

Satellites are incapable of directly measuring surface solar radiation. Instead, they measure the outgoing radiation at the top of atmosphere across specific spectral bands. This signal is substantially influenced by clouds, enabling the derivation of cloud cover or cloud optical depth from these measurements. Clear-sky surface solar radiation is estimated through physical modelling, which involves radiative transfer simulations using atmospheric water vapor, ozone and aerosols as input parameters. Water vapor and ozone data are sourced exclusively from ERA5 reanalysis data provided by ECMWF. The cloud information, retrieved directly from satellite radiances, is then employed to adjust the modelled clear-sky surface solar radiation to obtain the estimates of all-sky surface solar radiation. CM SAF's satellite algorithm GeoSatClim calculates both all-sky (SIS) and clear-sky (SISCF) surface solar radiation. It also provides the unique opportunity of two options regarding the aerosol input. The surface solar radiation can be simulated using modelled aerosol input with long-term variability, denoted as "CMIP" (since these aerosol data align with those utilized in models participating in CMIP6), or employing a daily aerosol climatology, labelled as "CLIM". Additionally, a dataset excluding the direct effect of water vapor on SIS, labelled as "noWV", can be generated. Combining these options differently allows the separation of cloud, direct aerosol and water vapor effects. This feature is the key that enables conducting the current study. GeoSatClim processes the corresponding datasets for all required combinations of the mentioned options for clouds, aerosol input and water vapor influence. It returns instantaneous values at intervals of 15 or 30 minutes (depending on the satellite generation, MVIRI or SEVIRI respectively) for the specific grid cell corresponding to the input coordinates.

These computations span the period 1983/01/01 to 2020/21/31. The specific locations and their corresponding input coordinates are listed in Appendix A. A total of 61 locations in Europe were subject to analysis.

For this study, a novel multiple linear regression model incorporating clouds, aerosols and water vapor as predictor variables was developed. The cloud signal was calculated as the ratio of all-sky radiation to clear-sky radiation, using time-varying aerosols both times as depicted by Equation 1. The water vapor signal was computed as the ratio of radiation with water vapor influence to radiation unaffected by water vapor directly using the time-varying aerosol input, as represented by Equation 2. The aerosol signal was determined as the ratio of all-sky radiation calculated using time-varying aerosols to all-sky radiation obtained using the aerosol climatology. It is described by Equation 3.

$$Clouds_t = \frac{SIS_t}{SISCF_t} \tag{1}$$

$$Water.vapor_t = \frac{SIS_t}{SIS.noWV_t} \tag{2}$$

$$Aerosols_t = \frac{SIS_t}{SIS.CLIM_t} \tag{3}$$

For each of the three signals, deseasonalized relative anomalies were computed. This effectively removes a significant portion of the seasonal variability. In Equations 4 to 7, S, C, A and W denote the logarithmic forms of the relative deseasonalized anomalies of SIS, Clouds, Aerosols and Water.vapor, respectively. These variables serve as the primary predictors of the regression model. The logarithm transformation is essential to compensate for the inherent skewness in the distribution of the ratios, thereby ensuring a theoretical condition for linear regression.

$$S = ln(\frac{SIS_t}{SIS_0}) \tag{4}$$

$$C = ln(\frac{Clouds_t}{Clouds_0}) \tag{5}$$

$$A = ln(\frac{Aerosols_t}{Aerosols_0}) \tag{6}$$

$$W = ln(\frac{Water.vapor_t}{Water.vapor_0}) \tag{7}$$

Relative anomalies have the advantage of allowing a better spatial and seasonal intercomparison. However, it should be taken into account that during winter satellite-based cloud detection encounters increased challenges, primarily attributable to the visual similarity between cloud cover and snow. Any erroneous cloud identification during this season significantly influences the observed relative brightening due to the lower radiation levels.

To account for seasonality, harmonic functions of first (Equations 8 and 9) and second (Equations 10 and 11) generation were included for the cloud, the aerosol and the water vapor predictor, as well as for the intercept (indicated with $_{\text{int}}$).

$$cos1 = cos((\frac{2\pi}{12}) \cdot month) \tag{8}$$

$$sin1 = sin((\frac{2\pi}{12}) \cdot month) \tag{9}$$

$$cos2 = cos((\frac{2\pi}{6}) \cdot month) \tag{10}$$

$$sin2 = sin((\frac{2\pi}{6}) \cdot month) \tag{11}$$

Adding an interactional component between clouds and water vapor as another predictor slightly improved the model further.

The final model, as represented by Equation 12, incorporates all aforementioned components, including an error term ϵ comprising residuals. This model attributes the identified trend in SIS (Equation 4) to the specific predictors. Individual model runs were performed for all locations. Assessment of the model's goodness of fit involved the calculation of the adjusted R-squared. Across all examined locations, an adjusted R-squared exceeding 95% was attained, with the majority exceeding 97%. These exceptionally high values indicate the model's capability to explain the variability in surface solar radiation.

$$\begin{aligned} S(t) = \; & \theta_{\text{int}} + \theta_{\text{int,cos1}} \cdot \cos 1 + \theta_{\text{int,sin1}} \cdot \sin 1 + \theta_{\text{int,cos2}} \cdot \cos 2 + \theta_{\text{int,sin2}} \cdot \sin 2 + \\ & C(t) \cdot (\theta_C + \theta_{C,\cos 1} \cdot \cos 1 + \theta_{C,\sin 1} \cdot \sin 1 + \theta_{C,\cos 2} \cdot \cos 2 + \theta_{C,\sin 2} \cdot \sin 2) + \\ & A(t) \cdot (\theta_A + \theta_{A,\cos 1} \cdot \cos 1 + \theta_{A,\sin 1} \cdot \sin 1 + \theta_{A,\cos 2} \cdot \cos 2 + \theta_{A,\sin 2} \cdot \sin 2) + \\ & W(t) \cdot (\theta_W + \theta_{W,\cos 1} \cdot \cos 1 + \theta_{W,\sin 1} \cdot \sin 1 + \theta_{W,\cos 2} \cdot \cos 2 + \theta_{W,\sin 2} \cdot \sin 2) + \\ & WxC(t) \cdot \theta_{WxC} + \epsilon(t) \end{aligned} \tag{12}$$

Linear trends in the main predictors (A, C, W, and their interactional term WxC) and the predictand (S) were computed for each month of the year, denoted as β_x for variable x. To ascertain the contribution of the individual effects (A, C, W, and WxC) in each month of the year, β was multiplied by the best estimate of the regression model denoted by θ, while considering the inclusion of four harmonics for A, C, and W. The example below focuses on the aerosol parameter, yet it is analogous for both the clouds and water vapor parameters.

$$\Lambda_A = \beta_A \cdot (\theta_A + \theta_{A,cos1} \cdot cos1 + \theta_{A,sin1} \cdot sin1 + \theta_{A,cos2} \cdot cos2 + \theta_{A,sin2} \cdot sin2) \tag{13}$$

The part in brackets can be summarized to θ_{tot}. Λ_A is the relative trend contribution of A for the respective month for A being in the logarithmic form.

$$\Lambda_A = \beta_A \cdot \theta_{A,tot} \tag{14}$$

In the framework of the global brightening analysis, the slope is the focus of investigation. Equation 15 shows the respective equation excluding the intercept. β_ϵ represents the trend in the residuals.

$$\beta_S = \beta_A \cdot \theta_{A,tot} + \beta_C \cdot \theta_{C,tot} + \beta_W \cdot \theta_{W,tot} + \beta_{WxC} \cdot \theta_{WxC} + \beta_\epsilon \tag{15}$$

The natural logarithm was introduced for all terms in the regression equation. Its mathematical elimination was necessary, in order to be able to properly interpret the outcome. Equation 15 was multiplied with $dt = t_2 - t_1$ in order to determine the period over which the relative trend is calculated. β_S indicates how large the relative difference (the factorial change) in SIS between t_1 and t_2 is. $dt = t_2 - t_1 = 10$ years represents the relative decadal difference. The equation is presented in its exponential form in Equation 16.

$$exp(\beta_S \cdot dt) = exp(\beta_A \cdot \theta_{A,tot} \cdot dt + \beta_C \cdot \theta_{C,tot} \cdot dt + \beta_W \cdot \theta_{W,tot} \cdot dt + \beta_{WxC} \cdot \theta_{WxC} \cdot dt + \beta_\epsilon \cdot dt) \tag{16}$$

Equation 16 can be rearranged to Equation 17. The terms become multiplicative.

$$\begin{aligned} \exp(\beta_S \cdot dt) = & (\exp(\beta_A \cdot dt))^{\theta_{A,\text{tot}}} \cdot (\exp(\beta_C \cdot dt))^{\theta_{C,\text{tot}}} \cdot (\exp(\beta_W \cdot dt))^{\theta_{W,\text{tot}}} \\ & \cdot (\exp(\beta_{WxC} \cdot dt))^{\theta_{WxC}} \cdot \exp(\beta_\epsilon \cdot dt) \end{aligned} \tag{17}$$

Equation 18 expresses the relative change in SIS over time dt.

$$\frac{SIS_{t2}}{SIS_{t1}} = exp(\beta_S \cdot dt) \tag{18}$$

Equation 19 expresses the relative change in global radiation SIS that was caused by changes in aerosols over time dt. It goes likewise for the other predictors (Equations 20 to 22).

$$\frac{Aerosols_{t2}}{Aerosols_{t1}} = exp(\beta_A \cdot dt) \tag{19}$$

$$\frac{Clouds_{t2}}{Clouds_{t1}} = exp(\beta_C \cdot dt) \tag{20}$$

$$\frac{Water.vapor_{t2}}{Water.vapor_{t1}} = exp(\beta_W \cdot dt) \tag{21}$$

$$exp(\frac{WxC_{t2}}{WxC_{t1}}) = exp(\beta_{WxC} \cdot dt) \tag{22}$$

Equation 17 can be expressed in an alternative manner.

$$\begin{aligned}\frac{SIS_{t2}}{SIS_{t1}} = &\left(\frac{Aerosols_{t2}}{Aerosols_{t1}}\right)^{\theta_{A,\text{tot}}} \cdot \left(\frac{Clouds_{t2}}{Clouds_{t1}}\right)^{\theta_{C,\text{tot}}} \cdot \left(\frac{Water.vapor_{t2}}{Water.vapor_{t1}}\right)^{\theta_{W,\text{tot}}} \\ &\cdot \left(\exp\left(\frac{WxC_{t2}}{WxC_{t1}}\right)\right)^{\theta_{WxC}} \cdot \left(\frac{\epsilon_{t2}}{\epsilon_{t1}}\right)\end{aligned} \tag{23}$$

The resulting factors presented on the right-hand side of Equation 23 represent the relative contributions of the respective parameters for the analyzed month. These factors signify the relative trends in SIS, assuming all other effects exhibited no trend (i.e., if the β's of all other effects were zero). These components denote factorial changes with a value of 1 indicating no trend in SIS. Values less than 1 suggest that the effect would lead to dimming rather than brightening during that month. The product of all factorial changes yields the relative change in SIS for the corresponding month of the year. These values represent the relative contributions over the time interval $t_2 - t_1 = dt$ years (dt = 10 years for relative decadal trend contributions) compared to the initial state in 1983/01/01. This calculation was performed for all months of the year across all 61 locations individually. Additionally, the 95% confidence interval was estimated for the cloud, the aerosol and the water vapor effects. They are based solely on the uncertainty of the estimated coefficients and were calculated for every locations separately using the bootstrap method and subsequently averaged over the respective locations as presented in Figures 6 and 8. To derive a final contribution per effect per location, the 12 monthly contributions were subsequently averaged. The intended design sought negative values for negative effects; therefore, 1 was subtracted from all values. These 12 values were then weighted by their corresponding climatological mean SIS (SIS_0), as contributions in summer exert a greater impact on the total effect due to the higher solar elevation and therefore increased radiation during this season. After being weighted by SIS_0 and averaged over the year, a single value was obtained and mapped onto the European map for all locations under consideration.

It is important to note that for the calculation of the individual contributions in the two sub-periods (Sections 4.2.2 and 4.2.3) the estimated coefficients (θ's) of the full period (1983/01/01 to 2020/12/31) were utilized, with only the β's extracted from the shortened sub-periods. This approach is justified by the understanding that the model's sensitivity to predictors remains consistent across various time scales – as it is of physical nature – with interannual estimates being representative of decadal trends. Therefore, the sensitivity of the model does not change for the sub-periods and utilizing estimates over a longer period ensures greater accuracy.

4 Results and Discussion

4.1 Validation of Satellite Dataset

The spatial analysis of the performance of GeoSatClim is shown in Figure 1. At many locations we find only very small trends of the bias compared to ground stations, which is a very

good result and proves the stability of the satellite-derived data. At most Central European locations, GeoSatClim exhibits a slight overestimation of the trend (blue) compared to ground stations, with the majority of locations showing bias trends below 3 W/m^2/dec. It demonstrates that the decadal trends observed from ground stations and satellite-derived data agree remarkably well over the British Isles, and particularly in Switzerland, where it yields highly stable values (very small trends in the bias). In Switzerland, the performance of the satellite-based GeoSatClim retrievals remains outstanding, even in high-elevation locations in the Alps. However, GeoSatClim notably underestimates the trend in surface solar radiation over the Iberian Peninsula, with deviations reaching up to -4 W/m^2/dec. Similar discrepancies between satellite and station data for the Iberian Peninsula have been previously observed by Pfeifroth et al. (2018) and Trentmann and Pfeifroth (2023), albeit for slightly different time periods. Trentmann and Pfeifroth (2023) concluded that these deviations might stem from erroneous station data.

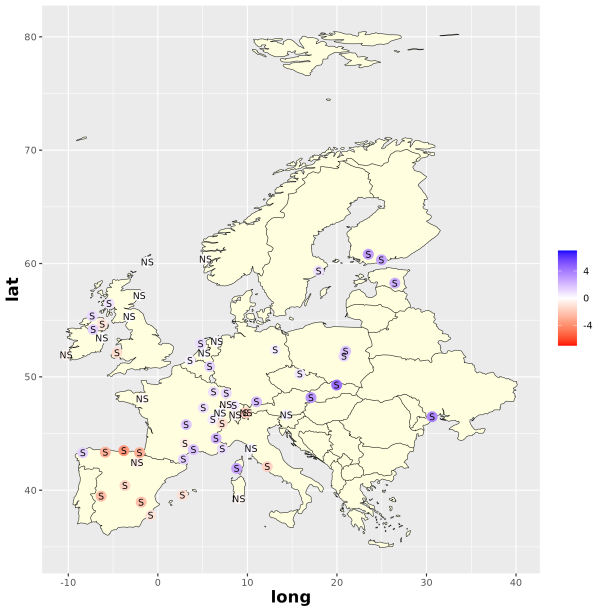

Figure 1: Bias of trends in surface solar radiation anomalies for GeoSatClim using time-varying aerosols (W/m^2/dec) compared to station data (GEBA and SMN). Positive/negative trends (blue/red) indicate that the satellite dataset is overpredicting/underpredicting the observed station trends. S = statistically significant trend (p-value < 0.05), NS = statistically not significant trend (p-value > 0.05).

The comprehensive findings depicted in Figure 1 reveal significant trends of the bias at numerous locations and a distinct spatial pattern. In stability analysis, the preference typically lies with non-significant trends. Nonetheless, the presence of significant trends does not necessarily imply poor performance of the algorithm, as significant trends can occur quickly in regression analysis conducted on time series data with many data points.

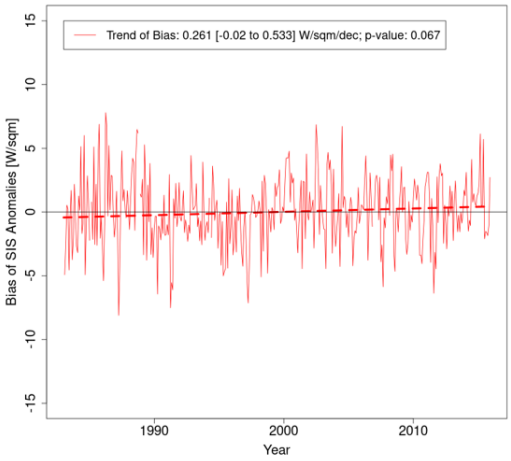

Figure 2: Biases (compared to GEBA and SMN data) of monthly surface solar radiation anomalies for GeoSatClim CMIP (W/m^2) averaged over all 61 locations in Europe. Additionally shown is the linear decadal trend of the biases (dashed straight line) in W/m^2/dec. The values in brackets represent the 95% confidence interval of the estimated trend.

Averaging across all locations yields a stability measure of 0.3 W/m^2/dec (as shown in Figure 2), meaning, that on average the satellite-derived data overestimated the trend observed from ground stations by 0.3 W/m^2/dec. This is a commendable result indicative of GeoSatClim's reliability. However, the spatial distribution observed in Figure 1 needs further consideration. Over- and underestimation of the brightening (blue and red points, respectively) partially offset each other across Europe. Nevertheless, the analysis substantiates the stability of GeoSatClim data throughout Europe. We therefore have confidence in the trend analysis.

Figure 3 illustrates the deseasonalized monthly and annual mean surface solar radiation anomalies, including the linear decadal Mann-Kendall trends (Mann-Kendall test, (Mann, 1945; Kendall, 1975)), separately averaged over the 53 locations outside of Switzerland and over the 8 locations within Switzerland. For the average of the 53 non-Swiss stations, a mean trend of 2.6 W/m^2/dec is found when using GEBA reference data. GeoSatClim, utilizing time-varying aerosols (CMIP), shows a trend of 3.3 W/m^2/dec. Hence, GeoSatClim overestimates this trend by 0.7 W/m^2/dec (in comparison to the GEBA reference). Conversely, employing the aerosol climatology (CLIM), GeoSatClim significantly underestimates it by 1.7 W/m^2/dec. All calculated trends exhibit statistical significance with very low p-values. The mean absolute bias (MAB) when using time-varying aerosols is 5 W/m^2, while it is 5.4 W/m^2 when employing the aerosol climatology.

The average of the 8 Swiss locations derived from SMN station data is 2.5 W/m^2/dec. GeoSatClim calculates a linear trend of 2.4 W/m^2/dec when utilizing time-varying aerosols, reaffirming the exceptional data quality of GeoSatClim in Switzerland. As expected, when employing an aerosol climatology, the observed trends cannot be reproduced (0.9 W/m^2/dec). This underscores the critical importance of using time-varying aerosols instead of a constant climatology. The MAB is 6.1 W/m^2 using the time-varying aerosols and 6.5 W/m^2 using the climatology.

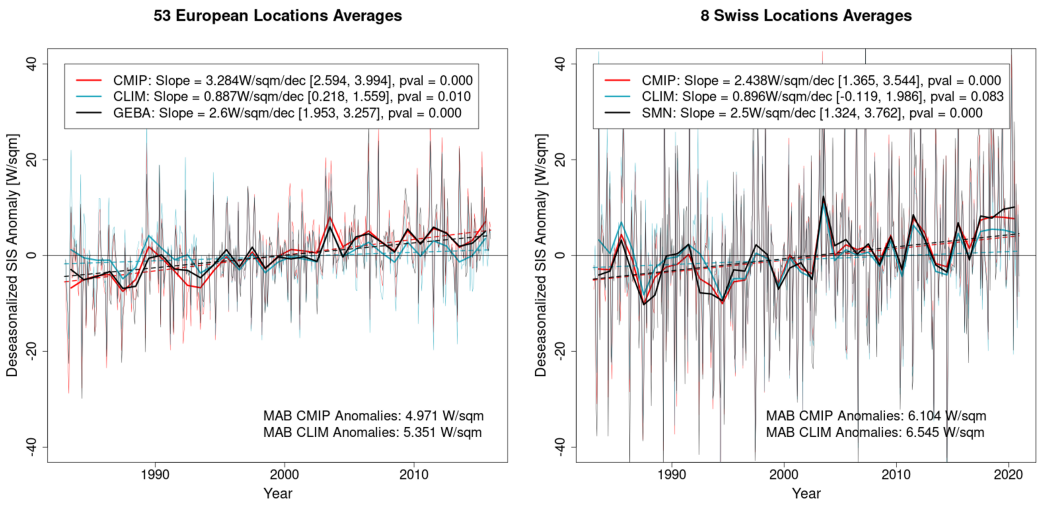

Figure 3: Monthly (thin lines) and annual (bold lines) mean surface solar radiation anomalies (W/m^2) of the 53 locations outside of Switzerland for the period 1983/01/01 to 2015/12/31 and the 8 locations in Switzerland for the period 1983/01/01 to 2020/12/31. Additionally shown are the linear trends (dashed straight lines). CMIP = GeoSatClim using time-varying aerosols (red), CLIM = GeoSatClim using the aerosol climatology (blue), GEBA/SMN = GEBA/SMN stations reference data (black), pval = p-value. The values in brackets show the 95% confidence interval of the estimated trends. Furthermore, the mean absolute biases (MAB) of the deseasonalized anomalies are shown.

4.2 Brightening and Contributions

4.2.1 Full Period 1983 to 2020

Across Europe, a consistent brightening is observed over the period 1983/01/01 to 2020/12/31, where satellite data are available, with the most pronounced values evident in Eastern and North-Eastern Europe (see Figure 4). Conversely, the smallest values are detected over the British Isles, the Iberian Peninsula and the Alpine regions in the southern part of Switzerland. Regarding the aerosol effect, minimal spatial variability is visible, except for the negligible aerosol effect at the four high-elevation locations in southern Switzerland and the marginally higher values in Eastern Europe (up to 3%/dec). However, the majority of locations showed aerosol effects between 1 and 2%/dec. The relatively lower values observed in Southern Europe could potentially be attributed to an enhanced influence of natural aerosol particles such as Saharan dust. Governmental regulations aimed at reducing emissions would not have affected the natural aerosol particle load. The nearly absent aerosol effect at higher altitudes is expected, as most sources that emit aerosol particles are located close to the Earth' surface, resulting in lower aerosol loads at higher elevations.

The cloud effect shows a more intricate spatial pattern. It tends to be slightly negative (dimming-inducing) in Northern Spain and at certain locations in the British Isles, with values ranging mostly from 0 to -2%/dec. Conversely it is predominantly positive everywhere else, ranging from 1 to 3%/dec at most locations, with the highest magnitudes observed at higher latitude locations. Notably, at high-altitude locations in Switzerland the cloud effect tends to be negligible.

The water vapour effect and also the interactional term between clouds and water vapor resulted negligible at all considered locations. Therefore, these effects are not shown. As both presented effects, the aerosol and the cloud effect, appear very similar when analyzing the whole period, we decided to split the period. The two sub-periods are analyzed separately and the find-

380 ings are presented in the following two sections. More detail regarding the sensitivity of the pe-
381 riod split can be found in Section 1 and in the Supplementary Material Figures S1 to S6.

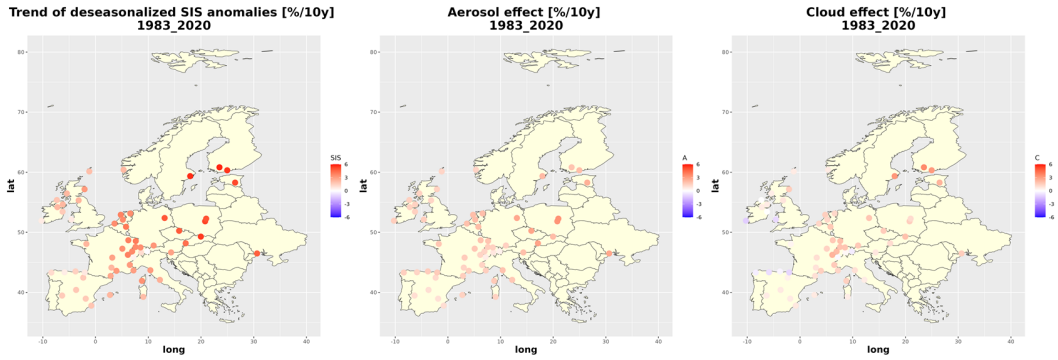

Figure 4: Relative changes in SIS (brightening) and relative cloud and aerosol effects per decade (%/dec) averaged over all months of the year and weighted according to their climatological mean surface solar radiation over the period 1983/01/01 to 2020/12/31. All data shown in this figure are satellite-derived.

382 ### *4.2.2 Sub-period 1983 to 2002*

383 A widespread brightening is found, when analyzing the sub-period 1983 to 2002 (see Fig-
384 ure 5). Despite also observing a brightening across Europe, notable differences in the aerosol and
385 cloud effects are evident in this sub-period compared to the full period. The aerosol effect is pos-
386 itive throughout Europe, predominantly ranging between 2 and 4%/dec, with the highest values
387 in Eastern Europe, reaching up to 6%/dec. The high-altitude locations (Swiss Alpine locations)
388 display only negligible aerosol effects, while values over the Iberian Peninsula also remain min-
389 imal (ranging from 0 to 1%/dec). The cloud effect reveals a distinct pattern. It is negative (dimming-
390 inducing) across most locations, with values ranging from -3 to -2%/dec for the majority of an-
391 alyzed locations. At selected locations, the cloud effect reaches magnitudes of -4 to -5%/dec. Pos-
392 itive values are only found in northern regions (around 2%/dec) and around the Mediterranean
393 Sea (ranging from 0 to 2%/dec), contributing to a brightening in these areas.

394 The overall aerosol effect remains positive at all locations also for the shortened period,
395 indicating a widespread brightening attributed to the overall trend in AOD. Chiacchio et al. (2011)
396 examined AOD trends in Europe for the period 1979 to 2007 estimated by the Goddard Chem-
397 istry Aerosol Radiation and Transport model (GOCART) and they found decreasing AOD across
398 the continent, which explains the positive values obtained. Particularly in Eastern Europe, a re-
399 gion known for its industrial activity, substantial aerosol effects are found. These effects can po-
400 tentially be attributed to successful implementation of emission regulations or also to the decline
401 of heavy industry following the dissolution of the Soviet Union in 1991 (Ohvril et al., 2009). Apart
402 from Eastern Europe, the strongest trends are observed in Central/Northern Europe, while the
403 weakest trends are observed in Southern Europe and at high altitudes (the four southern Swiss
404 locations). A likely explanation for this pattern are the lower aerosol loads at higher elevations
405 and the larger surface solar radiation values at lower latitudes, which make relative effects smaller.
406 This pattern is elucidated in more detail in Section 4.2.1. Regarding the cloud effect, Norris and
407 Wild (2007) reported a slight increase in cloud cover during the period 1987 to 2002. Further anal-
408 ysis by Sanchez-Lorenzo et al. (2017) focused on summer cloud cover trends from 1983 to 2009,
409 revealing a positive trend in cloud cover for the summer months across Central Europe, Eastern
410 Europe, and most of the British Isles, which supports the findings of the current study. Analyz-
411 ing the period 1981 to 2005, Ruckstuhl et al. (2010) concluded that cloud optical depth increased
412 in all seasons, with more pronounced trends in winter. These findings align with this study's pre-

dominantly negative cloud effects (causing dimming) for this first sub-period. Additionally, Stjern et al. (2009) emphasized the role of the cloud effect in North-Eastern and Arctic Europe in driving the detected brightening. Consistently, the present study also identifies a positive cloud effect conducive to a brightening in North-Eastern Europe, however alongside an equally prominent positive aerosol effect in these regions.

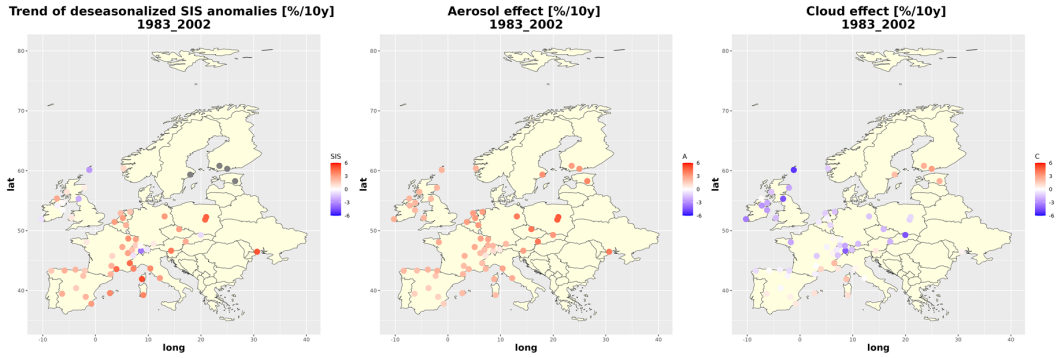

Figure 5: Relative changes in SIS (brightening) and relative cloud and aerosol effects per decade (%/dec), averaged over all months of the year and weighted according to their climatological mean surface solar radiation over the period 1983/01/01 to 2002/12/31. All data shown in this figure are satellite-derived.

Figure 6 shows the seasonality of the contributors to the observed decadal trends in surface solar radiation, averaged across all locations, as well as specifically over the ten most northern and ten most southern locations spanning from 1983/01/01 to 2002/12/31. Values exceeding 1.00 indicate a positive effect on the surface solar radiation trend, thereby inducing a brightening, while values below 1.00 signify that the corresponding effect induced a dimming during the respective time of the year. For instance, a value of 1.07 refers to an effect responsible for a brightening of 7 %/dec in the corresponding month of the year, assuming no other effects were present. The product of all trend contributions equals the satellite surface solar radiation trend calculated using time-varying aerosols.

Even when considering the average over all 61 locations (see the corresponding plot in Figure 6), seasonality is discernible. The relative brightening is positive throughout the year except for July and October to December, with its zenith observed in the first half of the year, particularly in January and May (both peaking around 6%/dec), and in August (around 3%/dec). This result confirms previous analyses by Chiacchio and Wild (2010) and Sanchez-Lorenzo et al. (2017), who found, based on in situ observations, that the European brightening is most pronounced in spring and summer. However, while their focus was on absolute brightening, this study delves into relative brightening. Given the diminished solar elevation in winter, even a modest absolute brightening in W/m^2 can translate to a substantial relative brightening in %, thus explaining the January peak in the averaged plot across all locations. The consistently positive aerosol effect across all months suggests a reduction of AOD in all months of the year. The aerosol effect exhibits slight seasonality, peaking in winter months and maximally increasing surface solar radiation by around 4%/dec. It is known, that in Europe the absolute values of AOD are highest in summer (Filonchyk et al., 2020; Remer et al., 2008), as in winter there is increased precipitation washing aerosol particles out of the atmosphere. Consequently, an identical AOD decrease throughout all months of the year results in the largest relative values in winter, which could explain the minor visible seasonality of the aerosol effect. However, the AOD is predominated by anthropogenic aerosol particles, subject to stringent emission controls. This also suggests limited variability, although seasonality could still be apparent due to for example stronger heating in winter. In contrast, the cloud effect demonstrates much stronger seasonality than the aerosol effect.

With negligible seasonality in the aerosol effect and negligible contributions from other terms, the cloud effect drives the seasonal variation of the brightening. Peaks in cloud effect occur in May (4%/dec) and August (0%/dec), while negative effects in July and later months indicate increased cloud cover and/or cloud optical depth over time during these months. The water vapor effect and interactional term appear irrelevant.

All months considered, the aerosol effect emerges as the predominant driver of the brightening on average, with the cloud effect contributing most to its seasonality. In several months, the cloud effect decreased surface solar radiation trends, but still a brightening resulted, as the cloud-induced dimming was overpowered by the aerosol-induced brightening. The narrow 95% confidence interval shows the very small uncertainty of the calculated contributions. This uncertainty refers only to the uncertainty in the estimated coefficients (see Section 3 for details). It is small for the aerosol effect, with slightly larger uncertainty in winter months. For the water vapour effect it is barely visible at all and for the cloud effect it is so small, that it coincides with the best estimate and is not visible at all in Figure 6.

Examining the additional plots in Figure 6 depicting averages over the ten most northern and southern locations reveals differences compared to the average over all locations. At more northern latitudes, the aerosol effect appears slightly stronger and its seasonality is more pronounced. The cloud effect also exhibits greater seasonal variability, peaking in March, May and most prominently in September. Conversely, southern locations exhibit weaker aerosol effects and less pronounced seasonality. However, this decreased seasonality of the aerosol effect (almost constant throughout the year) could also be due to the relative nature of the analysis and generally higher SIS values at lower latitudes. The cloud effect also shows less seasonality, with particularly similar values throughout spring and summer. A solitary strong cloud peak is visible in February. The uncertainty of the aerosol effect is larger for the average of the 10 most northern locations, but again it is rather small.

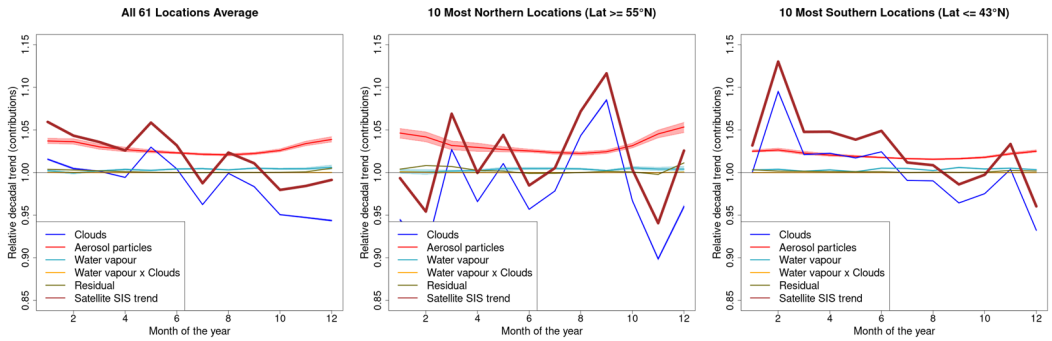

Figure 6: Monthly contributions to the brightening by effect as per regression model for the period 1983/01/01 to 2002/12/31 including the 95% confidence interval. Mean values of all 61 considered locations, mean of the 10 northern-most locations with latitude $\geq$ 55°N and mean of the 10 southern-most locations with latitude $\leq$ 43°N are shown. Additionally shown in colored shading are the 95% confidence intervals of the aerosol, the cloud and the water vapor effects. Satellite SIS trend (thick brown): Decadal trend of the relative surface solar radiation anomalies from GeoSatClim using time-varying aerosols (cMIP).

4.2.3 Sub-period 2001 to 2020

The brightening that was observed in the previous sub-period persists in this sub-period (see Figure 7). At many locations it even intensified. When analyzing the aerosol and cloud effects, a notable difference from the corresponding plots of the earlier sub-period 1983/01/01 to

2002/12/31 (Figure 5) is evident. During this later period, the aerosol effect exhibits minimal to negligible influence across all locations, ranging from 0 to 1%/dec. In contrast, the cloud effect demonstrates a more substantial, predominantly positive impact on SIS trends. Particularly pronounced cloud effects are observed in Central and Northern Europe, ranging from 2 to 5%/dec. The high-altitude locations in the Swiss Alps show only minimal cloud effects around 1%/dec.

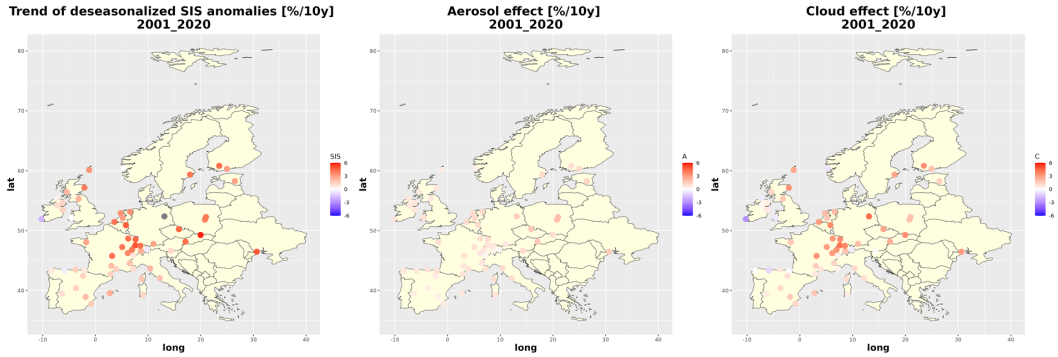

Figure 7: Relative changes in SIS (brightening) and relative cloud and aerosol effects per decade (%/dec), averaged over all months of the year and weighted according to their climatological mean surface solar radiation over the period 2001/01/01 to 2020/12/31. All data shown in this figure are satellite-derived.

During this second sub-period, the aerosol effect appears to exert only a minimal impact on the SIS trends, while the cloud effect emerges as a significant driver, exerting a dominant influence on the observed brightening across Europe. The regulative measures regarding anthropogenic emissions have started to be put in place in the 1980s and this study proves their at least partial success. As the emission levels were already reduced and the measures in place at the start of this sub-period analysis (2001/01/01), the decrease in AOD was rather small during the next 20 years, as resulted in the very small aerosol effects visible in Figure 7. Nevertheless, the brightening persisted during this period (ranging from 2 to 6%/dec), predominantly attributable to variations in cloudiness, as indicated by the pronounced cloud effects in Figure 7. This suggests a decrease in cloud optical depth and/or in total cloud cover over this period. The latter assertion finds support in the findings of Hatzianastassiou et al. (2020), who noted decreasing total cloud cover over Europe from 2001 to 2009. Their analysis, which also examined the individual contributions of total cloud cover and AOD to the observed brightening, concluded on clouds being the primary driver, with AOD exerting a minor influence (Figure 4 in Hatzianastassiou et al. (2020)). Similarly, Mateos et al. (2014) observed a dominant cloud effect when analyzing SIS trend contributions over the Iberian Peninsula from 2003 to 2012. Moreover, Ferreira Correa et al. (2023) noted the growing importance of the cloud radiative effect over the entire brightening period. All these findings are consistent with the results of the current study.

Figure 8 presents the seasonal evolution of the various contributors to the decadal SIS trends for the second sub-period. Notably, the cloud effect and the brightening exhibit striking similarities, appearing almost identical for certain months in both the northern and southern averaged plots. At the northern locations much higher winter values of SIS and cloud effect with a strong peak in January are found. A less pronounced, but very similar seasonality is found at southern latitudes, showing three smaller peaks in January, May and October. The aerosol effect remains low and displays minimal seasonality for all locations. No discernible effects are attributed to water vapor or the interactional term. Although the 95% confidence interval is included in Figure 8, it is barely visible for any of the effects. This underlines the accuracy of the estimated contributions, especially in this second sub-period.

When compared to the corresponding plots of the first sub-period (Figure 6), significant disparities emerge. Despite strong seasonality in the cloud effect, particularly evident at northern locations, it does not align with the seasonality observed in the sub-period 1983 to 2002. Instead, the first two decades of the 21st century are characterized by heightened relative cloud effects in winter across all locations and negligible to slightly negative cloud effects during the summer months. A potential reason for the observed discrepancies might be the change in Northern Atlantic Oscillation (NAO) regime around the change of century (Weisheimer et al., 2017; Papritz & Grams, 2018; Climate Prediction Center, 2024; National Weather Service - NOAA, 2024).

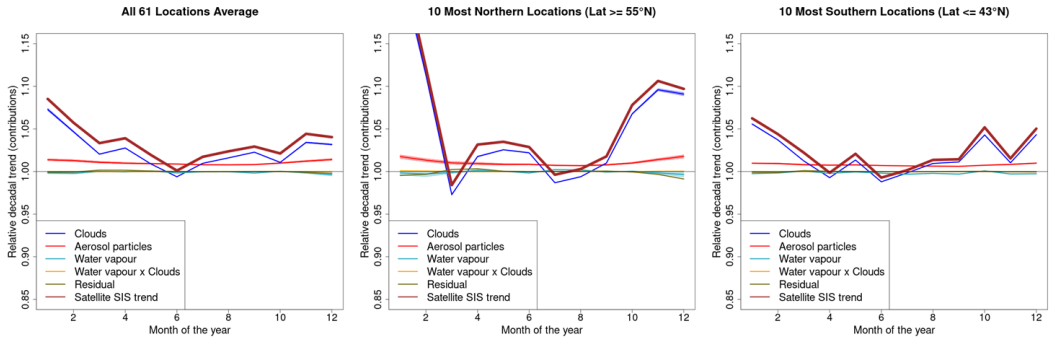

Figure 8: Monthly contributions to the brightening by effect as per regression model for the period 2001/01/01 to 2020/12/31 including the 95% confidence interval. Mean values of all 61 considered locations, mean of the 10 northern-most locations with latitude $\geq$ 55°N and mean of the 10 southern-most locations with latitude $\leq$ 43°N are shown. Additionally shown in colored shading are the 95% confidence intervals of the aerosol, the cloud and the water vapor effects. Satellite SIS trend (thick brown): Decadal trend of the relative surface solar radiation anomalies from GeoSatClim using time-varying aerosols (cMIP).

5 Conclusions

The aim of this study was to analyze and quantify the factors influencing the observed trends in surface solar radiation over the period 1983/01/01 to 2020/12/31 across 61 European locations. Initially, the satellite-derived data generated using the CM SAF GeoSatClim algorithm were validated against ground measurements obtained from GEBA and Swiss Met Net at the 61 locations. Subsequently, a detailed seasonal-scale analysis was conducted utilizing a multiple linear regression model to assess the individual contributions of clouds, aerosols, and water vapor to the observed brightening. CM SAF's Land Flux satellite algorithm offers flexibility to compute both all-sky and clear-sky radiation. Additionally, GeoSatClim provides two distinct options concerning aerosol input: CMIP, representing a simulation incorporating time-varying modelled aerosol optical depth, and CLIM, which utilizes a daily aerosol climatology with no long-term trend in aerosol optical depth. Moreover, the algorithm provides the option to eliminate the direct effect of water vapour on surface solar radiation.

The validation process for GeoSatClim utilizing time-varying aerosols revealed a robust alignment of trends with reference data across Europe, particularly in Switzerland, encompassing even its high-elevation Alpine regions. Generally, GeoSatClim exhibited a slight tendency to overestimate trends, with an exception observed in Spain, where trends were underestimated. As discussed in Section 4.1, potential discrepancies in the reference data from Spanish ground stations may account for this deviation.

Over the entire period 1983/01/01 to 2020/12/31 a brightening was found. Delving into the monthly-scale contributions to surface solar radiation trends yielded insightful findings. Ex-

amining this whole period revealed a balanced scenario, with nearly equal impacts stemming from variations in aerosol optical depth and cloudiness. Consequently, the period was split in two and each sub-period was analyzed individually.

For the first sub-period 1983/01/01 to 2002/12/31 a strong brightening was found and the aerosol effect emerged as the primary driver across Europe. The aerosol effect was particularly pronounced in Eastern Europe, while registering near-zero influence at high-altitude Alpine locations. This outcome resonates with findings by Chiacchio et al. (2011), who found a decline in aerosol optical depth across Europe between 1979 and 2007, based on results from an Atmospheric Chemistry Transport model, likely attributable to effective emission regulations. The intensified aerosol effects in Eastern Europe may be further linked to the decline of heavy industry following the dissolution of the Soviet Union in 1991 (Ohvril et al., 2009). Given that most aerosol-emitting sources are situated near the Earth's surface, resulting in lower aerosol optical depths at higher elevations, the minimal aerosol effect observed at Alpine locations is understandable. Clouds overall even increased during this sub-period and consequently exerted a negative impact on surface solar radiation trends at most locations, particularly in Central/Eastern Europe and in the British Isles. The contribution of water vapor remained negligible. As the aerosol effect overcompensated the negative cloud effect at most locations, it resulted in a brightening nonetheless. The uncertainties of the estimated contributions were small for the aerosol effect with larger uncertainty in winter months. The water vapor and cloud effects exhibited negligible uncertainty.

The analysis of the period 2001/01/01 to 2020/12/31 portrayed a substantially different situation. While the brightening persisted, the underlying contributors underwent notable shifts. The direct aerosol effect became rather insignificant, albeit still maintaining a positive influence. This suggests that anthropogenic aerosol emissions had likely reached regulatory thresholds and remained relatively stable during this latter sub-period. Variability in cloud cover, however, emerged as the predominant driver of the observed brightening in this sub-period. This study thus also enabled the detection of a substantial decrease in the cloud radiative forcing over Europe in the first two decades of the 21st century. Further exploration into the reasons of this decrease would complement the findings of this study. The water vapor effect was again negligible. Analyzing each month of the year separately revealed different seasonality for both investigated sub-periods. This is mainly attributable to the changed seasonality of the cloud effect, which could be a consequence of the Northern Atlantic Oscillation regime change. The uncertainties of the estimated coefficients were even smaller for this sub-period.

There are several limitations which should be kept in mind regarding this study. The spatial resolution of the satellite limits the accuracy, particularly in heterogeneous terrain, as it provides averaged values per grid cell. Consequently, very high-altitude locations such as mountain peaks were excluded from this study to mitigate potential inaccuracies. Another source of uncertainty stems from the aerosol optical depth data utilized, which was modelled and, from 2015/01/01 onwards, forced according to the socio-economic emission pathway SSP2-45, which is known to underestimate the actual changes (Schwalm et al., 2020). While the statistical regression model employed in this study has demonstrated excellent fidelity in reproducing satellite-observed surface solar radiation variability, residual model uncertainty persists. Regarding the interpretations of the findings, it is imperative to acknowledge that the aerosol effect discussed herein is the direct aerosol effect, wherein aerosol particles directly scatter and absorb incoming solar radiation. However, there exist additional indirect aerosol effects, whereby an increased number of aerosol particles increase the number of cloud droplets, because the particles act as cloud condensation nuclei. Increasing numbers of cloud droplets enhance the cloud's albedo, which amplifies the cooling effect of these clouds (Twomey et al., 1984). Apart from the described first indirect aerosol effect, aerosol particles can further prolong a cloud's lifespan by minimizing precipitation (Albrecht, 1989). The two indirect aerosol effects could not be analyzed separately with the available data, as they were encompassed within the cloud effect.

In recent years there have been studies conducted, analyzing correlations between long-term surface solar radiation trends and atmospheric circulation (Sanchez-Lorenzo et al., 2008; Chiacchio & Wild, 2010; Parding et al., 2016). There are also studies suggesting aerosol-cloud

591 interactions could depend on the level of pollution (Koren et al., 2008; Rosenfeld et al., 2008).
592 It could be of high interest to conduct further research in these directions.

593 Appendix A List of Locations

594 Table A1 lists all 61 locations that are analyzed in this study. Additionally to the station
595 name, the coordinates and the corresponding country are listed.

Table A1: List of 61 analyzed locations

Station	Longitude (°E)	Latitude (°N)	Country
Aberdeen	-2.08	57.17	Great Britain
Aberporth	-4.57	52.13	Great Britain
Ajaccio	8.80	41.92	France
Albacete	-1.86	38.95	Spain
Aldergrove	-6.22	54.65	Great Britain
Basel-Binningen	7.58	47.55	Switzerland
Belsk	20.78	51.83	Poland
Bergen	5.32	60.40	Norway
Bratislava	17.10	48.17	Slovak Republic
Caceres	-6.34	39.47	Spain
Cagliari	9.05	39.25	Italy
Clermont_ferrand	3.17	45.78	France
Clones	-7.23	54.18	Ireland
Col-du-Grand-St-Bern	7.17	45.87	Switzerland
Coruna	-8.38	43.30	Spain
Davos	9.85	46.82	Switzerland
Debilt	5.18	52.10	Netherlands
De_kooy	4.78	52.92	Netherlands
Dijon	5.08	47.27	France
Dublin	-6.25	53.43	Ireland
Dunstaffnage	-5.43	56.47	Great Britain
Eelde	6.58	53.13	Netherlands
Embrun	6.50	44.57	France
Eskdalemuir	-3.20	55.32	Great Britain
Geneve-Cointrin	6.13	46.25	Switzerland
Guetsch-Andermatt	8.62	46.65	Switzerland
Helsinki	24.97	60.32	Finland
Hohenpeissenberg	11.02	47.80	Germany
Hradec_kralove	15.85	50.25	Czech Republic
Jokioinen	23.50	60.82	Finland
Klagenfurt	14.33	46.65	Austria
Lerwick	-1.18	60.13	Great Britain
Logrono	-2.33	42.45	Spain
Maastricht	5.78	50.91	Netherlands
Madrid	-3.68	40.41	Spain
Malin_head	-7.33	55.37	Ireland
Millau	3.02	44.12	France
Montpellier	3.97	43.58	France
Murcia	-0.80	37.79	Spain
Nancy-essey	6.22	48.68	France
Nice	7.20	43.65	France
Odessa	30.63	46.48	Ukraine
Oviedo	-5.87	43.35	Spain

Continued on the next page

Table A1 – Continued from previous page

Station	Longitude (°E)	Latitude (°N)	Country
Palma_mallorca	2.74	39.57	Spain
Payerne	6.94	46.81	Switzerland
Perpignan	2.87	42.73	France
Pisa	10.40	43.68	Italy
Potsdam	13.10	52.38	Germany
Rennes	-1.73	48.07	France
San_sebastian	-2.04	43.31	Spain
Santander	-3.80	43.49	Spain
Stockholm	17.95	59.35	Sweden
Strasbourg	7.63	48.55	France
Toravere	26.47	58.27	Estonia
Valentia	-10.25	51.93	Ireland
Vigna_di_valle	12.21	42.08	Italy
Vlissingen	3.60	51.45	Netherlands
Warszawa	20.98	52.27	Poland
Weissfluhjoch	9.80	46.83	Switzerland
Zakopane	19.97	49.28	Poland
Zuerich-Kloten	8.53	47.48	Switzerland

Open Research Section

The Surface Radiation Climate Data Record will be available soon under the DOI `10.5676/EUM_SAF_CM/SLF_METEOSAT/V001`. The part of the data that was used for this study is temporarily available at `https://figshare.com/s/50f58aa738aadf53bfa6` for peer review.
Global Energy Balance Archive (GEBA) data is publicly accessible via `http://www.geba.ethz.ch` (Wild et al. (2017), supplementary data are available at `https://doi.org/10.1594/PANGAEA.873078`).
The reference data from the Swiss measurement stations (Swiss Met Net) are freely available upon request to MeteoSwiss via the contact form: `https://www.meteoswiss.admin.ch/about-us/contact/contact-form.html`.
The CAMS AOD re-analysis data is available under (`https://ads.atmosphere.copernicus.eu/cdsapp#!/dataset/cams-global-reanalysis-eac4-monthly?tab=form`.
The information about the aerosol optical depth is taken from model-based estimates that include pre-industrial natural aerosol and emission estimates (Fiedler, Kinne, et al., 2019) and information on different emission scenarios (Fiedler, Stevens, et al., 2019). For more details see Section 2.1.

Acknowledgments

This study is supported by MeteoSwiss and we thank them for the raw data supply. We extend our appreciation to Christoph Frei for his comprehensive statistical support concerning the definition, testing and application of the statistical model. He played a pivotal role in ensuring a robust analytical framework. We also thank Christian Grams for his valuable inputs regarding atmospheric regimes. The Global Energy Balance Archive (GEBA) is co-funded by the Federal Office of Meteorology and Climatology MeteoSwiss within the framework of GCOS Switzerland and we acknowledge Pascalle Smith for providing the GEBA data. Furthermore, we acknowledge Jörg Trentmann and Uwe Pfeifroth for the valuable discussions and their inputs.

References

Albrecht, B. A. (1989). Aerosols, Cloud Microphysics, and Fractional Cloudiness. *Science*, *245*(4923), 1227-1230. Retrieved from https://www.science.org/doi/abs/10.1126/science.245.4923.1227 doi: https://doi.org/10.1126/science.245.4923.1227

Bourgeois, Q., & Duguay-Tetzlaff, A. (2023). Algorithm Technical Base Document. Meteosat Surface Radiation Budget Edition 1. CM SAFCM SAF (www.cmsaf.eu to be published 11/2023).

Cano, D., Monget, J.-M., Albuisson, M., Guillard, H., Regas, N., & Wald, L. (1986). A method for the determination of the global solar radiation from meteorological satellite data. *Solar energy*, *37*(1), 31–39.

Chiacchio, M., Ewen, T., Wild, M., Chin, M., & Diehl, T. (2011). Decadal variability of aerosol optical depth in Europe and its relationship to the temporal shift of the North Atlantic Oscillation in the realm of dimming and brightening. *Journal of Geophysical Research: Atmospheres*, *116*(D2). Retrieved from https://agupubs.onlinelibrary.wiley.com/doi/abs/10.1029/2010JD014471 doi: https://doi.org/10.1029/2010JD014471

Chiacchio, M., & Wild, M. (2010). Influence of NAO and clouds on long-term seasonal variations of surface solar radiation in Europe. *Journal of Geophysical Research: Atmospheres*, *115*(D10). Retrieved from https://agupubs.onlinelibrary.wiley.com/doi/abs/10.1029/2009JD012182 doi: https://doi.org/10.1029/2009JD012182

Climate Prediction Center. (2024). *North Atlantic Oscillation.* Retrieved from https://www.cpc.ncep.noaa.gov/data/teledoc/nao.shtml

Dong, B., Sutton, R. T., & Wilcox, L. J. (2023). Decadal trends in surface solar radiation and cloud cover over the North Atlantic sector during the last four decades: drivers and physical processes. *Climate Dynamics*, *60*, 2533 – 2546. doi: https://doi.org/10.1007/s00382-022-06438-3

Ferreira Correa, L., Folini, D., Chtirkova, B., & Wild, M. (2023). Causes for decadal trends in Surface Solar Radiation in the Alpine region. *Authorea Preprints*.

Fiedler, S., Kinne, S., Huang, W. T. K., Räisänen, P., O'Donnell, D., Bellouin, N., ... Lohmann, U. (2019). Anthropogenic aerosol forcing – insights from multiple estimates from aerosol-climate models with reduced complexity. *Atmospheric Chemistry and Physics*, *19*(10), 6821–6841. Retrieved from https://acp.copernicus.org/articles/19/6821/2019/ doi: https://doi.org/10.5194/acp-19-6821-2019

Fiedler, S., Stevens, B., Gidden, M., Smith, S. J., Riahi, K., & van Vuuren, D. (2019). First forcing estimates from the future CMIP6 scenarios of anthropogenic aerosol optical properties and an associated Twomey effect. *Geoscientific Model Development*, *12*(3), 989–1007. Retrieved from https://gmd.copernicus.org/articles/12/989/2019/ doi: https://doi.org/10.5194/gmd-12-989-2019

Filonchyk, M., Hurynovich, V., Yan, H., Zhou, L., & Gusev, A. (2020). Climatology of aerosol optical depth over Eastern Europe based on 19 years (2000–2018) MODIS TERRA data. *International Journal of Climatology*, *40*(7), 3531-3549. Retrieved from https://rmets.onlinelibrary.wiley.com/doi/abs/10.1002/joc.6412 doi: https://doi.org/10.1002/joc.6412

Folini, D., & Wild, M. (2011). Aerosol emissions and dimming/brightening in Europe: Sensitivity studies with ECHAM5-HAM. *Journal of Geophysical Research: Atmospheres*, *116*(D21). Retrieved from https://agupubs.onlinelibrary.wiley.com/doi/abs/10.1029/2011JD016227 doi: https://doi.org/10.1029/2011JD016227

Foukal, P., Fröhlich, C., Spruit, H., & Wigley, T. M. L. (2006). Variations in solar luminosity and their effect on Earth's climate. *Nature*, *443*, 161–166. doi: https://doi.org/10.1038/nature05072

Gilgen, H., Roesch, A., Wild, M., & Ohmura, A. (2009). Decadal changes in shortwave ir-

radiance at the surface in the period from 1960 to 2000 estimated from Global Energy Balance Archive Data. *Journal of Geophysical Research: Atmospheres*, *114*(D10). Retrieved from https://agupubs.onlinelibrary.wiley.com/doi/abs/10.1029/2008JD011383 doi: https://doi.org/10.1029/2008JD011383

Gilgen, H., Wild, M., & Ohmura, A. (1998). Means and Trends of Shortwave Irradiance at the Surface Estimated from Global Energy Balance Archive Data. *Journal of Climate*, *11*(8), 2042 - 2061. Retrieved from https://journals.ametsoc.org/view/journals/clim/11/8/1520-0442_1998_011_2042_matosi_2.0.co_2.xml doi: 10.1175/1520-0442(1998)011<2042:MATOSI>2.0.CO;2

Hatzianastassiou, N., Ioannidis, E., Korras-Carraca, M.-B., Gavrouzou, M., Papadimas, C. D., Matsoukas, C., ... Vardavas, I. (2020). Global Dimming and Brightening Features during the First Decade of the 21st Century. *Atmosphere*, *11*(3). Retrieved from https://www.mdpi.com/2073-4433/11/3/308 doi: 10.3390/atmos11030308

Inness, A., Ades, M., Agustí-Panareda, A., Barré, J., Benedictow, A., Blechschmidt, A.-M., ... Suttie, M. (2019). The CAMS reanalysis of atmospheric composition. *Atmospheric Chemistry and Physics*, *19*(6), 3515–3556. Retrieved from https://acp.copernicus.org/articles/19/3515/2019/ doi: https://doi.org/10.5194/acp-19-3515-2019

Jacobson, M. Z., & Delucchi, M. A. (2011). Providing all global energy with wind, water, and solar power, Part I: Technologies, energy resources, quantities and areas of infrastructure, and materials. *Energy Policy*, *39*(3), 1154-1169. Retrieved from https://www.sciencedirect.com/science/article/pii/S0301421510008645 doi: https://doi.org/10.1016/j.enpol.2010.11.040

Julsrud, I. R., Storelvmo, T., Schulz, M., Moseid, K. O., & Wild, M. (2022). Disentangling Aerosol and Cloud effects on Dimming and Brightening in Observations and CMIP6. *Journal of Geophysical Research: Atmospheres*, *127*(21), e2021JD035476. Retrieved from https://agupubs.onlinelibrary.wiley.com/doi/abs/10.1029/2021JD035476 (e2021JD035476 2021JD035476) doi: https://doi.org/10.1029/2021JD035476

Kendall, M. G. (1975). Rank correlation methods. 2nd impression. *Charles Griffin and Company Ltd. London and High Wycombe*.

Koren, I., Vanderlei Martins, J., Remer, L. A., & Afargan, H. (2008). Smoke Invigoration Versus Inhibition of Clouds over the Amazon. *Science*, *321*(5891), 946-949. Retrieved from https://www.science.org/doi/abs/10.1126/science.1159185 doi: 10.1126/science.1159185

Liepert, B. G., Fabian, P., & Grassl, H. (1994). Solar radiation in Germany-observed trends and an assessment of their causes. Pt. 1; Regional approach. *Beitraege zur Physik der Atmosphaere;(Germany)*, *67*(1).

Liepert, B. G., Feichter, J., Lohmann, U., & Roeckner, E. (2004). Can aerosols spin down the water cycle in a warmer and moister world? *Geophysical Research Letters*, *31*(6). Retrieved from https://agupubs.onlinelibrary.wiley.com/doi/abs/10.1029/2003GL019060 doi: https://doi.org/10.1029/2003GL019060

Liepert, B. G., & Romanou, A. (2005). Global dimming and brightening and the water cycle.

Manara, V., Brunetti, M., Celozzi, A., Maugeri, M., Sanchez-Lorenzo, A., & Wild, M. (2016). Detection of dimming/brightening in Italy from homogenized all-sky and clear-sky surface solar radiation records and underlying causes (1959-2013). *Atmospheric Chemistry and Physics*, *16*(17), 11145–11161. Retrieved from https://acp.copernicus.org/articles/16/11145/2016/ doi: https://doi.org/10.5194/acp-16-11145-2016

Mann, H. B. (1945). Nonparametric tests against trend. *Econometrica*, *13*(3), 245–259. Retrieved 2023-08-09, from http://www.jstor.org/stable/1907187

Mateos, D., Sanchez-Lorenzo, A., Antón, M., Cachorro, V. E., Calbó, J., Costa, M. J., ... Wild, M. (2014). Quantifying the respective roles of aerosols and clouds in

the strong brightening since the early 2000s over the Iberian Peninsula. *Journal of Geophysical Research: Atmospheres*, *119*(17), 10,382-10,393. Retrieved from https://agupubs.onlinelibrary.wiley.com/doi/abs/10.1002/2014JD022076 doi: https://doi.org/10.1002/2014JD022076

Mueller, R. W., Matsoukas, C., Gratzki, A., Behr, H. D., & Hollmann, R. (2009). The CM-SAF operational scheme for the satellite based retrieval of solar surface irradiance—A LUT based eigenvector hybrid approach. *Remote Sensing of Environment*, *113*(5), 1012–1024.

Murphy, D. M., Solomon, S., Portmann, R. W., Rosenlof, K. H., Forster, P. M., & Wong, T. (2009). An observationally based energy balance for the Earth since 1950. *Journal of Geophysical Research: Atmospheres*, *114*(D17). Retrieved from https://agupubs.onlinelibrary.wiley.com/doi/abs/10.1029/2009JD012105 doi: https://doi.org/10.1029/2009JD012105

Nabat, P., Somot, S., Mallet, M., Sanchez-Lorenzo, A., & Wild, M. (2014). Contribution of anthropogenic sulfate aerosols to the changing Euro-Mediterranean climate since 1980. *Geophysical Research Letters*, *41*(15), 5605-5611. Retrieved from https://agupubs.onlinelibrary.wiley.com/doi/abs/10.1002/2014GL060798 doi: https://doi.org/10.1002/2014GL060798

NASA. (2016). *Forcings in GISS Climate Model.* Retrieved from https://data.giss.nasa.gov/modelforce/strataer/

National Weather Service - NOAA. (2024). *Observation of Monthly Mean North Atlantic Oscillation.* Retrieved from https://www.cpc.ncep.noaa.gov/products/precip/CWlink/pna/month_nao_index.shtml

Norris, J. R., & Wild, M. (2007). Trends in aerosol radiative effects over Europe inferred from observed cloud cover, solar "dimming," and solar "brightening". *Journal of Geophysical Research: Atmospheres*, *112*(D8). Retrieved from https://agupubs.onlinelibrary.wiley.com/doi/abs/10.1029/2006JD007794 doi: https://doi.org/10.1029/2006JD007794

Ohmura, A. (1989). Secular variation of global radiation in Europe. *IRS'88: Current problems in atmospheric radiation*, 298–301.

Ohvril, H., Teral, H., Neiman, L., Kannel, M., Uustare, M., Tee, M., ... Laulainen, N. (2009). Global dimming and brightening versus atmospheric column transparency, Europe, 1906–2007. *Journal of Geophysical Research: Atmospheres*, *114*(D10). Retrieved from https://agupubs.onlinelibrary.wiley.com/doi/abs/10.1029/2008JD010644 doi: https://doi.org/10.1029/2008JD010644

Padma Kumari, B., & Goswami, B. N. (2010). Seminal role of clouds on solar dimming over the Indian monsoon region. *Geophysical Research Letters*, *37*(6). Retrieved from https://agupubs.onlinelibrary.wiley.com/doi/abs/10.1029/2009GL042133 doi: https://doi.org/10.1029/2009GL042133

Papritz, L., & Grams, C. M. (2018). Linking Low-Frequency Large-Scale Circulation Patterns to Cold Air Outbreak Formation in the Northeastern North Atlantic. *Geophysical Research Letters*, *45*(5), 2542-2553. Retrieved from https://agupubs.onlinelibrary.wiley.com/doi/abs/10.1002/2017GL076921 doi: https://doi.org/10.1002/2017GL076921

Parding, K. M., Liepert, B. G., Hinkelman, L. M., Ackerman, T. P., Dagestad, K., & Olseth, J. A. (2016). Influence of synoptic weather patterns on solar irradiance variability in northern Europe. *Journal of Climate*, *29*(11), 4229 - 4250. Retrieved from https://journals.ametsoc.org/view/journals/clim/29/11/jcli-d-15-0476.1.xml doi: https://doi.org/10.1175/JCLI-D-15-0476.1

Pfeifroth, U., Sanchez-Lorenzo, A., Manara, V., Trentmann, J., & Hollmann, R. (2018). Trends and variability of surface solar radiation in Europe based on surface- and satellite-based data records. *Journal of Geophysical Research: Atmospheres*, *123*(3), 1735-1754. Retrieved from https://agupubs.onlinelibrary.wiley.com/doi/abs/10.1002/2017JD027418 doi: https://doi.org/10.1002/2017JD027418

Philipona, R., Behrens, K., & Ruckstuhl, C. (2009). How declining aerosols and rising greenhouse gases forced rapid warming in Europe since the 1980s. *Geophysical Research Letters*, *36*(2). Retrieved from https://agupubs.onlinelibrary.wiley.com/doi/abs/10.1029/2008GL036350 doi: https://doi.org/10.1029/2008GL036350

Remer, L. A., Kleidman, R. G., Levy, R. C., Kaufman, Y. J., Tanré, D., Mattoo, S., ... Holben, B. N. (2008). Global aerosol climatology from the MODIS satellite sensors. *Journal of Geophysical Research: Atmospheres*, *113*(D14). Retrieved from https://agupubs.onlinelibrary.wiley.com/doi/abs/10.1029/2007JD009661 doi: https://doi.org/10.1029/2007JD009661

Rosenfeld, D., Lohmann, U., Raga, G. B., O'Dowd, C. D., Kulmala, M., Fuzzi, S., ... Andreae, M. O. (2008). Flood or Drought: How Do Aerosols Affect Precipitation? *Science*, *321*(5894), 1309-1313. Retrieved from https://www.science.org/doi/abs/10.1126/science.1160606 doi: 10.1126/science.1160606

Ruckstuhl, C., Norris, J. R., & Philipona, R. (2010). Is there evidence for an aerosol indirect effect during the recent aerosol optical depth decline in Europe? *Journal of Geophysical Research: Atmospheres*, *115*(D4). Retrieved from https://agupubs.onlinelibrary.wiley.com/doi/abs/10.1029/2009JD012867 doi: https://doi.org/10.1029/2009JD012867

Ruckstuhl, C., Philipona, R., Behrens, K., Collaud Coen, M., Dürr, B., Heimo, A., ... Zelenka, A. (2008). Aerosol and cloud effects on solar brightening and the recent rapid warming. *Geophysical Research Letters*, *35*(12). Retrieved from https://agupubs.onlinelibrary.wiley.com/doi/abs/10.1029/2008GL034228 doi: https://doi.org/10.1029/2008GL034228

Sanchez-Lorenzo, A., Calbó, J., & Martin-Vide, J. (2008). Spatial and temporal trends in sunshine duration over Western Europe (1938–2004). *Journal of Climate*, *21*(22), 6089 - 6098. Retrieved from https://journals.ametsoc.org/view/journals/clim/21/22/2008jcli2442.1.xml doi: https://doi.org/10.1175/2008JCLI2442.1

Sanchez-Lorenzo, A., Calbó, J., & Wild, M. (2013). Global and diffuse solar radiation in Spain: building a homogeneous dataset and assessing their trends. *Global and Planetary Change*, *100*, 343-352. Retrieved from https://www.sciencedirect.com/science/article/pii/S0921818112002238 doi: https://doi.org/10.1016/j.gloplacha.2012.11.010

Sanchez-Lorenzo, A., Enriquez-Alonso, A., Wild, M., Trentmann, J., Vicente-Serrano, S. M., Sanchez-Romero, A., ... Hakuba, M. Z. (2017). Trends in downward surface solar radiation from satellites and ground observations over Europe during 1983–2010. *Remote Sensing of Environment*, *189*, 108-117. Retrieved from https://www.sciencedirect.com/science/article/pii/S0034425716304655 doi: https://doi.org/10.1016/j.rse.2016.11.018

Sanchez-Lorenzo, A., Wild, M., Brunetti, M., Guijarro, J. A., Hakuba, M. Z., Calbó, J., ... Bartok, B. (2015). Reassessment and update of long-term trends in downward surface shortwave radiation over Europe (1939–2012). *Journal of Geophysical Research: Atmospheres*, *120*(18), 9555-9569. Retrieved from https://agupubs.onlinelibrary.wiley.com/doi/abs/10.1002/2015JD023321 doi: https://doi.org/10.1002/2015JD023321

Schwalm, C. R., Glendon, S., & Duffy, P. B. (2020). RCP8.5 tracks cumulative CO_2 emissions. *Proceedings of the National Academy of Sciences*, *117*(33), 19656-19657. Retrieved from https://www.pnas.org/doi/abs/10.1073/pnas.2007117117 doi: https://doi.org/10.1073/pnas.2007117117

Stanhill, G., & Moreshet, S. (1992). Global radiation climate changes: The world network. *Climatic Change*, *21*(1), 57–75.

Stjern, C. W., Kristjánsson, J. E., & Hansen, A. W. (2009). Global dimming and global brightening — An analysis of surface radiation and cloud cover data in northern Europe. *International Journal of Climatology*, *29*(5), 643-653. Retrieved from

https://rmets.onlinelibrary.wiley.com/doi/abs/10.1002/joc.1735 doi: https://doi.org/10.1002/joc.1735

Stoeckli, R. (2017). The HelioMont surface solar radiation processing 2017 update. *Scientific Report MeteoSwiss*, *93*, 122.

Streets, D. G., Yan, F., Chin, M., Diehl, T., Mahowald, N., Schultz, M., ... Yu, C. (2009). Anthropogenic and natural contributions to regional trends in aerosol optical depth, 1980–2006. *Journal of Geophysical Research: Atmospheres*, *114*(D10). Retrieved from https://agupubs.onlinelibrary.wiley.com/doi/abs/10.1029/2008JD011624 doi: https://doi.org/10.1029/2008JD011624

Trentmann, J., & Pfeifroth, U. (2023). Assessing the quality of gridded Climate Data Records of the Surface Irradiance using global Reference Data Sets. *EGU General Assembly, Vienna, Austria, 24-28 Apr 2023, EGU23-2563*. doi: https://doi.org/10.5194/egusphere-egu23-2563

Twomey, S. A., Piepgrass, M., & Wolfe, T. L. (1984). An assessment of the impact of pollution on global cloud albedo. *Tellus B*, *36B*(5), 356-366. Retrieved from https://onlinelibrary.wiley.com/doi/abs/10.1111/j.1600-0889.1984.tb00254.x doi: https://doi.org/10.1111/j.1600-0889.1984.tb00254.x

Vestreng, V., Myhre, G., Fagerli, H., Reis, S., & Tarrasón, L. (2007). Twenty-five years of continuous sulphur dioxide emission reduction in Europe. *Atmospheric Chemistry and Physics*, *7*(13), 3663–3681. Retrieved from https://acp.copernicus.org/articles/7/3663/2007/ doi: https://doi.org/10.5194/acp-7-3663-2007

Weisheimer, A., Schaller, N., O'Reilly, C., MacLeod, D. A., & Palmer, T. (2017). Atmospheric seasonal forecasts of the twentieth century: multi-decadal variability in predictive skill of the winter North Atlantic Oscillation (NAO) and their potential value for extreme event attribution. *Quarterly Journal of the Royal Meteorological Society*, *143*(703), 917-926. Retrieved from https://rmets.onlinelibrary.wiley.com/doi/abs/10.1002/qj.2976 doi: https://doi.org/10.1002/qj.2976

Wild, M. (2009). Global dimming and brightening: A review. *Journal of Geophysical Research: Atmospheres*, *114*(D10). Retrieved from https://agupubs.onlinelibrary.wiley.com/doi/abs/10.1029/2008JD011470 doi: https://doi.org/10.1029/2008JD011470

Wild, M. (2012). Enlightening Global Dimming and Brightening. *Bulletin of the American Meteorological Society*, *93*(1), 27 - 37. Retrieved from https://journals.ametsoc.org/view/journals/bams/93/1/bams-d-11-00074_1.xml doi: https://doi.org/10.1175/BAMS-D-11-00074.1

Wild, M. (2016). Decadal changes in radiative fluxes at land and ocean surfaces and their relevance for global warming. *WIREs Climate Change*, *7*(1), 91-107. Retrieved from https://wires.onlinelibrary.wiley.com/doi/abs/10.1002/wcc.372 doi: https://doi.org/10.1002/wcc.372

Wild, M., Gilgen, H., Roesch, A., Ohmura, A., Long, C. N., Dutton, E. C., ... Tsvetkov, A. (2005). From dimming to brightening: Decadal changes in solar radiation at Earth's surface. *Science*, *308*(5723). doi: https://doi.org/10.1126/science.1103215

Wild, M., Ohmura, A., & Makowski, K. (2007). Impact of global dimming and brightening on global warming. *Geophysical Research Letters*, *34*(4). Retrieved from https://agupubs.onlinelibrary.wiley.com/doi/abs/10.1029/2006GL028031 doi: https://doi.org/10.1029/2006GL028031

Wild, M., Ohmura, A., Schär, C., Müller, G., Folini, D., Schwarz, M., ... Sanchez-Lorenzo, A. (2017). The Global Energy Balance Archive (GEBA) version 2017: A database for worldwide measured surface energy fluxes. *Earth System Science Data*, *9*(2), 601–613. Retrieved from https://essd.copernicus.org/articles/9/601/2017/ doi: https://doi.org/10.5194/essd-9-601-2017

Wild, M., Wacker, S., Yang, S., & Sanchez-Lorenzo, A. (2021). Evidence for Clear-Sky Dimming and Brightening in Central Europe. *Geophysical Research Letters*, *48*(6), e2020GL092216. Retrieved from https://agupubs.onlinelibrary.wiley.com/doi/abs/10.1029/2020GL092216 (e2020GL092216 2020GL092216)

doi: https://doi.org/10.1029/2020GL092216

Zerefos, C. S., Eleftheratos, K., Meleti, C., Kazadzis, S., Romanou, A., Ichoku, C., ... Bais, A. (2009). Solar dimming and brightening over Thessaloniki, Greece, and Beijing, China. *Tellus B: Chemical and Physical Meteorology*, *61*(4), 657-665. Retrieved from https://doi.org/10.1111/j.1600-0889.2009.00425.x doi: 10.1111/j.1600-0889.2009.00425.x

Zhou, L., Sun, L., Luo, Y., Xia, X., Huang, L., Liao, Z., & Yan, X. (2023). Air pollutant concentration trends in China: correlations between solar radiation, PM2.5, and O3. *Air Quality, Atmosphere and Health*, *16*, 1721 – 1735. doi: https://doi.org/10.1007/s11869-023-01368-3

Zou, L., Wang, L., Li, J., Lu, Y., Gong, W., & Niu, Y. (2019). Global surface solar radiation and photovoltaic power from Coupled Model Intercomparison Project Phase 5 climate models. *Journal of Cleaner Production*, *224*, 304-324. Retrieved from https://www.sciencedirect.com/science/article/pii/S0959652619309783 doi: https://doi.org/10.1016/j.jclepro.2019.03.268